

Journal of Biomedical Optics

SPIEDigitalLibrary.org/jbo

Methodological considerations for global analysis of cellular FLIM/FRET measurements

Nur Aida Abdul Rahim
Serge Pelet
Roger D. Kamm
Peter T. C. So

Methodological considerations for global analysis of cellular FLIM/FRET measurements

Nur Aida Abdul Rahim,^a Serge Pelet,^b Roger D. Kamm,^{a,b} and Peter T. C. So^{a,b}

^aMassachusetts Institute of Technology, Department of Mechanical Engineering, 77 Massachusetts Avenue, Cambridge, Massachusetts 02139

^bMassachusetts Institute of Technology, Department of Biological Engineering, 77 Massachusetts Avenue, Cambridge, Massachusetts 02139

Abstract. Global algorithms can improve the analysis of fluorescence energy transfer (FRET) measurement based on fluorescence lifetime microscopy. However, global analysis of FRET data is also susceptible to experimental artifacts. This work examines several common artifacts and suggests remedial experimental protocols. Specifically, we examined the accuracy of different methods for instrument response extraction and propose an adaptive method based on the mean lifetime of fluorescent proteins. We further examined the effects of image segmentation and a priori constraints on the accuracy of lifetime extraction. Methods to test the applicability of global analysis on cellular data are proposed and demonstrated. The accuracy of global fitting degrades with lower photon count. By systematically tracking the effect of the minimum photon count on lifetime and FRET prefactors when carrying out global analysis, we demonstrate a correction procedure to recover the correct FRET parameters, allowing us to obtain protein interaction information even in dim cellular regions with photon counts as low as 100 per decay curve. © 2012 Society of Photo-Optical Instrumentation Engineers (SPIE). [DOI: 10.1117/1.JBO.17.2.026013]

Keywords: Förster resonance energy transfer; fluorescence lifetime imaging; global analysis; mechanotransduction.

Paper 11244SS received May 17, 2011; revised manuscript received Dec. 18, 2011; accepted for publication Dec. 27, 2011; published online Mar. 19, 2012.

1 Introduction

The development of genetically encoded fluorescent proteins such as green fluorescent proteins (GFPs)¹ and variants^{2–5} greatly expands our capability to monitor protein interactions. To definitively detect protein binding, fluorescence energy transfer (FRET) is often utilized. Methods used to detect the presence of FRET include those based on 1. intensity measurements with various steps to correct for spectral bleed-through^{6,7}, 2. the acceptor photobleaching approach^{8,9}, 3. spectral imaging microscopy to measure a complete per pixel emission spectrum,^{10–12} 4. fluorescence polarization anisotropy measurements that compare the orientation of excited and emitting molecules,^{13–16} and 5. monitoring changes in donor or acceptor fluorescence lifetimes either in the time domain^{17–20} or in the frequency domain^{9,18,21–23} using fluorescence lifetime microscopy (FLIM).

Among these methods, FRET based on FLIM measurement of donor lifetime is relatively simple to implement and provides images with good signal-to-noise ratio. The fluorescence decay profile of donor fluorophore upon ultrafast pulse excitation is measured, and the shortening of the donor lifetime due to the occurrence of FRET via the donor-acceptor interaction can be calculated from this decay profile.²⁴ The major strength of FLIM measurements compared to intensity-based measurements is that they provide FRET parameters (i.e., energy transfer efficiency, interfluorophore distance, and ratio of bound to free donors) independently of fluorescence intensity or local probe concentration. However, processes such as donor photobleaching can still skew FRET measurement results. Furthermore, since magic angle condition cannot be realized in the typical

microscopy setting, FLIM may be affected by time-dependent polarization relaxation of the protein-bound fluorophores. When the increasing availability of commercial user-friendly systems for carrying out FLIM measurements²⁵ is also taken into consideration, it is no surprise that the number of FRET/FLIM papers published has increased in recent years.^{24,26}

Problems in the interpretation of FLIM-FRET data on the cellular level stem from the fact that the lifetimes of bound and free donors are often relatively close and must be resolved from donor decay curves that are noisy because of low photon counts. The closeness of the lifetimes depends on the efficiency of energy transfer: Accurate measurement of lifetimes that are closer together is more difficult.^{21,27,28} The requirement of minimal perturbation of intracellular conditions means that there is a trade-off between high photon counts required for a good signal level and low fusion protein concentration for physiologically relevant conditions. Therefore, it is important to formulate a methodology for extracting all the information present in these information-rich but noisy decay curves.

Many approaches have been developed to analyze and visualize FLIM data. Recently, the phasor approach has provided a power method to visualize the presence of FRET and estimate FRET parameters.^{21,29–31} Complementarily, the parameters of these decay curves can be extracted by objective function minimization, typically by using a mean squares measure. Many research groups have further shown that global analysis that simultaneously minimizes all decay curves from a particular image allow the extraction of physical parameters of interest with high precision. The strength of global analysis relies on the use of a priori information to significantly reduce the degrees of freedom in the fitting algorithm. It has been shown that global fitting of FLIM, assuming spatially invariant lifetimes, accurately

Address all correspondence to: Peter T. C. So, Massachusetts Institute of Technology, Department of Mechanical Engineering, 77 Massachusetts Avenue, Cambridge, Massachusetts 02139. E-mail: pts@mit.edu.

extracts two lifetimes, both for frequency-domain measurements^{22,32} and for time-domain measurements³³ when independent fitting of individual pixels fails. Although global analysis is a successful approach, it suffers from significant computational burden and can be relatively slow for analyzing large data sets typical of FLIM images. Recent work on computational efficiency improvement include analysis of data after Chebyshev transform³⁰ and the incorporation of image structure information.^{33,34}

Presented herein are methodological considerations for fitting time-domain FLIM data measured in cells to recover single lifetimes (τ_D) from samples without FRET, as well as the second lifetime (τ_F) and the fractions of interacting fluorophores from samples undergoing FRET using global analysis, specifically based on the image segmentation approach.³³ The reliability of quantifying instrument response is found to be critical for accurate global fitting of lifetime decay curves. We demonstrate an adaptive method for acquiring instrument responses to be used when fitting the decay curves. We further examine the applicability of global analysis and the segmentation approach for cell data. We analyze the dependence of the accuracy of lifetime fits on total photon counts. As an illustration, we apply these techniques to study the interaction of paxillin and the focal adhesion targeting (FAT) domain of focal adhesion kinase (FAK), which are cytosolic proteins that tend to localize to focal adhesions (FA) that are sites of cell attachment to the extracellular matrix and are implicated in a variety of mechanotransduction processes. Our samples consist of bovine aortic endothelial cells (BAECs) singly transfected with GFP-paxillin (without FRET) and cells cotransfected with GFP-paxillin (GPax) and FAT-mCherry (FATmCh) (with FRET).

2 Theory

2.1 FRET and FLIM

Upon the occurrence of FRET, donor fluorophores acquire an additional nonradiative decay pathway, which adds to the nonradiative rate constant and reduces lifetime. FLIM measurements can be carried out by exciting only donor fluorophores within the system. Fluorescence decay curves are collected on a per-pixel basis. For the study of interactions between proteins labeled with donor and acceptor fluorophores, the donor population consists of ones that are bound to acceptors and are undergoing FRET (FRETing) and free ones that are not undergoing FRET (nonFRETing). Therefore, in a FRET system with only one donor population and one acceptor population present, the total per-pixel fluorescence intensity decay measured is as follows:

$$I(t) = \int_0^t G(t-T)(\alpha_D e^{-T/\tau_D} + \alpha_F e^{-T/\tau_F})dT, \quad (1)$$

where $I(t)$ is a convolution of the sum of the exponentials with the instrument response $G(t)$. The preexponential factors α_D and α_F reflect fractional contributions to the total fluorescence from the FRETing and nonFRETing donor species, respectively, each of which undergoes decay at rates τ_D and τ_F . The prefactors are expressed in this paper in terms of $\alpha_F/(\alpha_D + \alpha_F)$, the ratio of FRETing donor to total donor and termed the ‘‘FRET ratio’’ (FR). The efficiency of the energy transfer process that occurs during FRET, E , can be written

in terms of lifetimes and also in terms of molecular separation between donor and acceptor, r :

$$E = 1 - \frac{\tau_F}{\tau_D} = \frac{1}{1 + \left(\frac{r}{R_0}\right)^6}. \quad (2)$$

R_0 , the Förster radius, is the interfluorophore distance when energy transfer is 50% efficient. R_0 depends on the donor quantum yield, Q_D , the overlap integral J , the orientation factor κ , and the index of refraction of the medium n :

$$R_0^6 = \frac{9000 \ln(10)\kappa^2 Q_D}{128 \pi^5 N_A n^4} J, \quad (3)$$

where J represents the overlap between donor emission and acceptor excitation spectrums, and κ is usually set to 2/3, representing a random relative orientation between the transition dipole of the donor and acceptor molecules. R_0 is on the order of 50 to 60 Å for well-matched fluorophore pairs.^{35,36}

2.2 Global Fitting Algorithm

The global fitting algorithm developed by Pelet et al.³³ is utilized to fit our fluorescence decay data to the model expressed as Eq. (1) above. In summary, decay curves are scaled to a maximum of one before fitting. The prefactors are bounded such that $(\alpha_D + \alpha_F) = 1$, but are allowed to vary spatially. It is assumed that only two fluorophores exist in each pixel, nonFRETing and FRETing species; thus the fitted lifetimes are spatially invariant. The least-squares estimate χ^2 is used as a merit function to optimize the values of all fit coefficients:

$$\chi^2 = \sum_i \sum_t \left\{ \frac{[I_i^{\text{model}}(t) - I_i^{\text{data}}(t)]^2}{I_i^{\text{data}}(t)} \right\}, \quad (4)$$

where $I_i^{\text{data}}(t)$ is the experiment data of the decay curve i as a function of time t and $I_i^{\text{model}}(t)$ is the model of the decay curve i as a function of time t . When fitting single-exponential decay curves, the same algorithm is used but with setting the prefactor α_F to zero.

Image segmentation was carried out based on intensity thresholding whereby pixels of similar intensities were grouped together and their decay curves summed. A global fit is performed on this very limited set of decay curves (segment-sum)³³ to obtain coefficients that were subsequently used as initial guesses in the final global fitting step (global-indiv). This method of using an educated initial guess of fit parameters was shown to greatly accelerate time to convergence.³³ It is possible to carry out segmentation because paxillin and FAT are cytosolic proteins that localize to FAs. Images obtained at the basal adhesion plane therefore capture the locations of FAs, which are more intense than the rest of the cell area and can be grouped together. Figure 1 shows intensity and segmented images of GPax-only and GPax/FATmCh cells.

Data fitting clearly depends on SNR level. Pixels with decay curves consisting of a minimum of 1000 photon counts are selected for fits unless otherwise specified. We express our lower limit (LL) in photon count symbolically as LL1000.

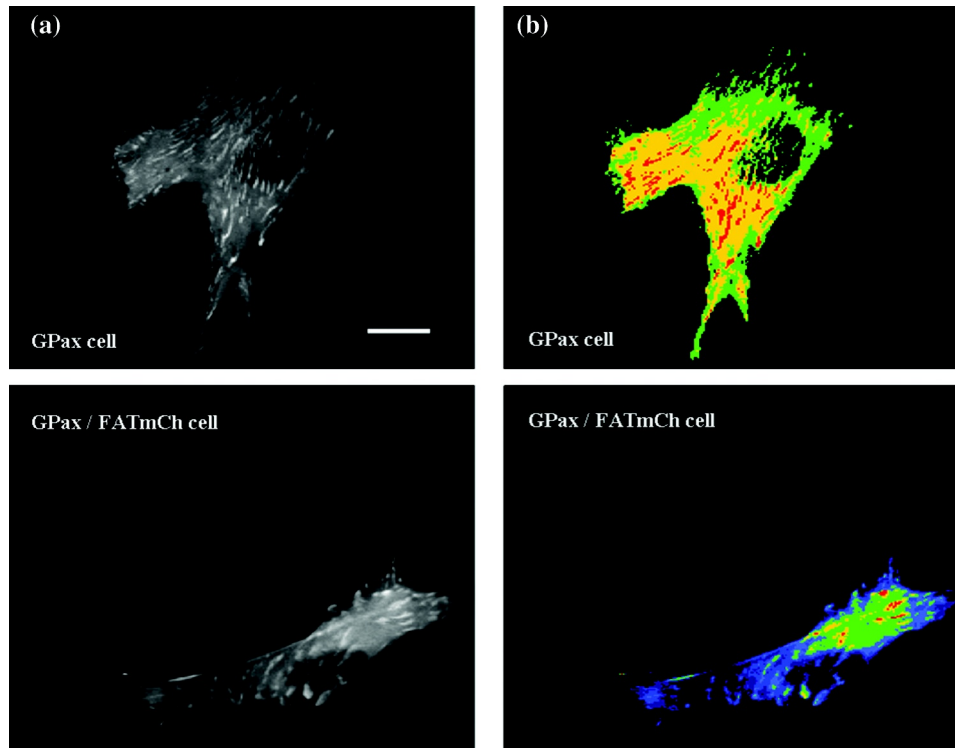


Fig. 1 (a) Fluorescence intensity images of GPax (top) and GPax/FATmCh (bottom) cells. (b) Images of the same cells in (a) segmented by intensity and arbitrarily colored to distinguish different intensity segments. Only pixels with LL1000 were selected for intensity segmentation. Scale bar is 10 μm .

3 Methods

3.1 Cell Preparation

BAECs were cultured in Dulbecco's Modified Eagle's Medium (DMEM) (Gibco/Invitrogen, Carlsbad, CA) supplemented with 10% fetal bovine serum, 1% penicillin/streptomycin, and 1% L-glutamine. Cells were seeded at an initial density of 160 000 cells/well in fibronectin-coated 35-mm glass-bottomed dishes (MatTek Corporation, Ashland, MA). Plasmids used for transfection were either GFP-paxillin (gift from K Yamada of the National Institutes of Health, Bethesda, MD) or FAT-mCherry. Mouse FAT from the dsRed-FAT plasmid (N. Mochizuki, National Cardiovascular Center Research Institute, Osaka, Japan) was amplified by polymerase chain reaction (PCR) with primer pairs (5'-CTAAGCAACCTGTCCAGCATCAGC-3') and (5'-CGGATCCGGGTGTGGCCGTGTCTGCCCTAGC-3'). The resulting PCR fragment was ligated into a pcDNA4/HisMax@ TOPO@ vector (Invitrogen, Carlsbad, CA). mCherry from the pRSET-B mCherry plasmid (R. Tsien, University of California San Diego) was digested with *EcoRI* and *BamHI* and ligated into the pcDNA4-FAT vector at the 3' end of FAT. The FAT-mCherry plasmid was amplified using the QIAGEN MaxiPrep kit (QIAGEN, Valencia, CA). Plasmid notation (GPax, FATmCh) indicates the position of fluorophore within the fusion protein, where GFP is at the N terminus of paxillin and mCherry is at the C terminus of FAT. Cells were transfected at $\approx 80\%$ confluence with either GFP-paxillin plasmids only or cotransfected with both GFP-paxillin and FAT-mCherry plasmids using the FuGENE 6 transfection reagent from Roche Diagnostics (Indianapolis, IN). Note that plasmid notation indicates the

position of the fluorophore within the fusion protein, where GFP is at the N terminus of paxillin and mCherry is at the C terminus of FAT. Lifetime imaging was carried out 24 h after transfection.

3.2 Optical Setup

Details of the two-photon lifetime imaging microscope setup have been described previously.^{18,33,37} In brief, a custom-built, two-photon microscope³⁷ was modified for obtaining lifetime images. This microscope is based on a modified inverted microscope, the Axiovert 110 by Zeiss (Göttingen, Germany), with a femtosecond laser source from the Mira family of mode-locked Ti:Sapphire oscillators by Coherent (80 MHz, 150 fs; Santa Clara, CA).^{18,33} The laser, tuned at 890 nm, excites a subfemtoliter volume at the focal point of a 40 \times Fluor lens objective (1.3 numerical aperture; Zeiss). Pixel images (256 \times 256 pixels) spanning a field of view of 120 \times 120 μm^2 were imaged with a pixel residence time between 25 and 200 μs , depending on specimen brightness. The fluorescence signal from the cell is first selected with a short-pass Schott BG-39 filter and a short-pass 700-nm filter from Chroma Technology Corporation (Rockingham, VT), which minimizes contributions from scattered light and autofluorescence, before being sent to the top port of the microscope, where it is filtered for green wavelengths with a HQ500LP emission filter from Chroma. A photomultiplier tube (PMT) (R7400P; Hamamatsu Bridgewater, NJ) detects emitted photons, and this signal is sent to a time-correlated single-photon counting (TCSPC) card (SPC-730; Becker-Hickl, Berlin, Germany).

3.3 FLIM Imaging

The instrument response (IR) of the system was measured using either fluorescein (flsn) in a well-slide or gallium arsenide (GaAs) dried onto a coverslip. Because flsn has a well-characterized decay of 4.0 ns,^{38,39} the IR can be extracted as a Gaussian that best fits the fluorescein decay curve with a preset decay time of 4.0 ns. For GaAs, the second harmonic generation (SHG) signal from the GaAs surface is instantaneous, thus directly giving us the IR.

Cells selected for FLIM imaging were those in the middle range of fluorescence intensities (corresponding to cells containing fluorophores with concentrations in the micromolar range) as observed using epifluorescence with a 488-nm argon ion laser (MWK Industries, Austin, TX) or a 432-nm diode laser (Laserglow Technologies, Toronto, Ontario, Canada). This is a compromise between ensuring a bright-enough cell that has sufficient photon counts for decay curves with acceptable SNR and cells that are not grossly overexpressing the fusion proteins, which could introduce artifacts into the interactions we wish to measure. The selected cells typically have fluorescent proteins with concentration in the nanomolar to micromolar levels. FLIM imaging of transfected cells would take 7 or 8 minutes. All FLIM imaging was carried out at 890 nm. At this wavelength, mCherry is minimally excited, with fluorescence levels within the noise range. The microscope was carefully focused to the basal adhesion plane of the cell before we carried out FLIM imaging.

3.4 Simulated Decay Curves

To test the conclusions derived from fitting of experimental data, sets of simulated decay curves, with Poisson noise added, were generated and fitted with the global fitting algorithm. Decay curves have either a single lifetime ($\tau_D = 2.6$ ns; single-exponential decay) or two lifetimes ($\tau_D = 2.6$ ns, $\tau_F = 1.3$ ns; double-exponential decay). For sets of decay curves containing two lifetimes, the prefactors within each set were varied such that $0 \leq \alpha_F / (\alpha_D + \alpha_F) \leq 1$. Each decay curve is convolved with a Gaussian instrument response of 0.25 ns, with Poisson noise added to simulate the photon-counting process. The total photon counts within decay curves were allowed to vary between

100 and 3000, consistent with typical experimental data and depending on the fitting method being tested.

3.5 Computation

The global fitting algorithm as developed by Pelet et al.³³ was carried out based on MATLAB (MathWorks, Natick, MA) and uses the MATLAB built-in *fmincon* optimization function. Convergence is defined as being reached when χ^2 varies by less than 10^{-15} .

4 Results

4.1 Instrument Response

One way to account for IR is to acquire SHG signal from a surface, GaAs in our case. Because SHG is instantaneous, this method directly gives us the IR. Another method would be to take FLIM data of a sample with a well-characterized lifetime, for example, flsn, which has a lifetime of 4.0 ns. Convolution of a Gaussian to a single-exponential decay of lifetime 4.0 ns and comparing this to the actual flsn data would recover the Gaussian that best depicts the IR. With either method, measurements of the IR (I_{msr}) would typically be taken before carrying out cell measurements, and it is assumed that the IR does not vary throughout the imaging session. However, a number of factors in TCSPC microscopy may contribute to substantial variations in I_{msr} , such as electronic circuit noise, or to laser instabilities. We found that the most difficult problem for some Ti:sapphire lasers is the sudden, unpredictable changes in IR that are sometimes observed. We attribute these changes to the losing and regaining of mode-locking of the laser. Representative variation in IR due to periodic laser instability is shown in Figure 2(a), where IR width varies by about 100 ps within just 1 to 2 minutes.

If the IR varies appreciably throughout the imaging session, it is inaccurate to use just one IR for all calculations. An adaptive approach that extracts IR directly from the image data is adopted for live-cell FRET imaging. Though it would be possible to interleave data collection from sample and reference specimens and collect IR data throughout the imaging session, this method is not very practical, as it significantly increases data acquisition time and perturbs the specimen, especially given that the IR

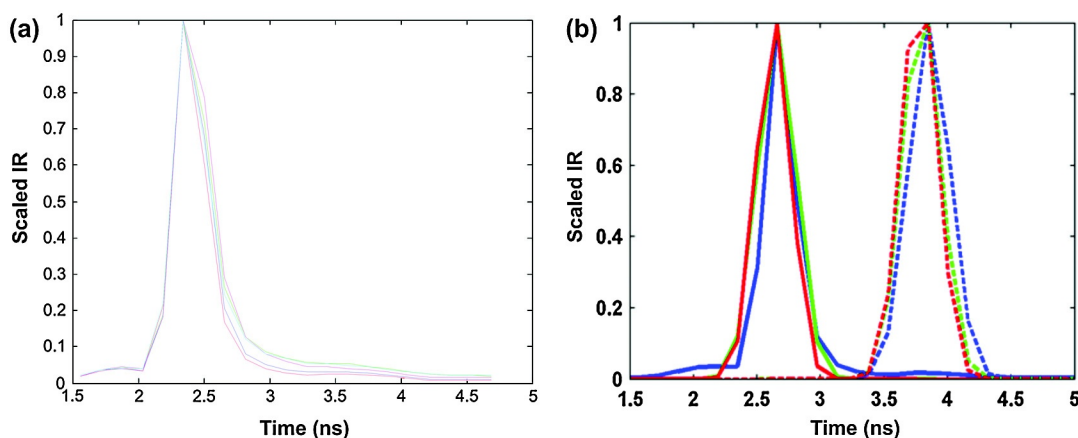


Fig. 2 (a) Four representative variations instrument response (IR) functions were taken over a period of 2 min. A width variation of over 100 ps was seen. (b) Scaled IRs for two data sets. For the solid line plot of data set 1, the blue line is $IR_{msr}(GaAs)$, the green line is $I_{Rext}(GPax)$, and the red line is $I_{Rext}(GPax)/FATmCh$. For the dashed line plot of data set 2, the blue line is $I_{Rext}(flsn)$, the green line is $I_{Rext}(GPax)$, and the red line is $I_{Rext}(GPax)/FATmCh$. The plot for data set 2 has been shifted to the right by 1.5 ns for clarity.

profile changes unpredictably. In contrast, an adaptive approach allows continuous recovery of IRs over time throughout the experiment, mitigating the issue of sudden IR jumps observed with mode-locked lasers.

To overcome this problem, an adaptive solution was developed based on the assumption that the mean lifetime can be readily extracted and is invariant for a homogeneous population of cells. Our approach is based on many prior works, and we have extended them in FRET studies.⁴⁰⁻⁴³ The IR is directly extracted from the cell FLIM data (IR_{ext}). All decay curves from every pixel of the image are summed, and the IR is calculated by presetting mean lifetimes of $\tau = 2.7$ ns for GPax-only cells and $\tau = 2.3$ ns for GPax/FATmCh cells. The Gaussian with full-width half-maximum (FWHM) varied that, once convolved with a single-exponential decay having the preset lifetime, best fits the master decay curve is used as the IR for that particular image. Variations in preset lifetimes of ± 0.3 ns produced negligible variations in the FWHM of the Gaussian IR (data not shown), thus validating our method of direct IR extraction. Since this approach is most useful in kinetic or long-term FRET study of protein interactions in live cells when interleaving live-cell and reference compound imaging is impractical, the required mean lifetime values for this adaptive algorithm can be readily measured as control experiments prior to critical studies by referencing to known lifetime standards.

A plot of scaled IR showing the difference between IR_{msr} and IR_{ext} for two data sets is given in Fig. 2(b). The dashed line plot compares differences between IR_{msr} from flsn and sample IR_{ext} from GPax and GPax/FATmCh cells, whereas the solid line plot compares differences between IR_{msr} from GaAs and sample IR_{ext} . Only very slight differences between different the IRs can be observed. However, these slight differences are sufficient to produce different fitted lifetime results, especially for double-exponential decays. This is shown in Table 1. When fitting single-exponential decays to GPax curves, both IR methods recover similar lifetimes. However, discrepancies become obvious when fitting double-exponential decays to data from double-transfected cells. Fits using both methods produce reasonable-looking fits (data not shown), and in all cases, the χ^2 has been minimized. However, fitting with IR_{msr} , the expected two FRET lifetimes cannot be reliably recovered for either GaAs or flsn. IR_{msr} GaAs recovered lifetimes of $\tau_D = 2.16 \pm 0.13$ ns and $\tau_F = 0.01$ ns, whereas IR_{msr} Flsn recovered lifetimes of $\tau_D = 2.30 \pm 0.10$ ns and $\tau_F = 0.01$ ns. In both cases, the recovered τ_D is an average of the two lifetimes recovered using IR_{ext} . In contrast, expected single- and double-exponential lifetimes can be obtained using IR_{ext} .

Our results demonstrate that to obtain two relevant FRET lifetimes from double-exponential decay curves, the IR used in fits is important. Because the IR varies throughout the imaging session for our setup, an IR measured at the start of the experiment is rendered invalid for use with data generated later within the imaging session. Even a slight variation in IR could cause deviations in fit results. Therefore, a more robust adaptive method is used to obtain IR_{ext} and obtain more consistent fits. IR_{ext} is used for all subsequent fits for both FRETing and nonFRETing decay curves.

Theoretically, the decision to use GFP lifetime as an internal reference for single transfected cells is well-justified because GFP exhibits a single-exponential decay that is relatively insensitive to the cellular environment. For double-transfected cells, the mean lifetime is used as a reference because it can be more robustly measured compared to quantifying a double-exponential decay with noisy data. It also relies on the assumption that the cellular population studied is biochemically homogeneous within biological noise and that its mean lifetime is invariant with time. Clearly, these assumptions cannot always be met in some studies, and this approach needs to be used with caution.

Finally, this approach is unsuited to extracting very short lifetime components, such as from second harmonic generation. However, with our focus on FRET studies where the quenched donors normally still have fairly long lifetimes (for GFP, lifetime shortens from 2.6 ns to 1.8 ns), this is not a major concern. Furthermore, if strong SHG, Raman or Rayleigh scattering is present, their contribution may be removed by modeling an additional zero lifetime component convoluted with IR.

4.2 Segmented and Global Fits

We examine the differences in lifetime fits observed between various fitting procedures and also between global fitting results from summed curves and individual curves. All fitting algorithms use the model represented by Eq. (1). For both GPax-only cells (eight cells) and GPax/FATmCh cells (five cells), fits were carried out with (i) a single-exponential decay, (ii) a double-exponential decay with τ_D fixed at 2.6 ns and (iii) both lifetimes freely varying. For each fitting procedure, results are compared between global fitting of individual decay curves carried out over the whole cell image (global-indiv) and global fitting of decay curves summed upon segmentation according to intensity thresholds (segment-sum) as previously described. LL1000 was chosen, which resulted in ≈ 8000 decays fit for global-indiv and ≈ 6 decays fit for segment-sum.

Table 1 Lifetimes obtained from fits of GPax-only cells and GPax/FATmCh cells using either IR_{msr} (flsn or GaAs) or IR_{ext} .

	IR_{msr} method	IR_{msr}		IR_{ext}		
		τ_D (ns)	τ_F (ns)	τ_D (ns)	τ_F (ns)	
Single-exponential (GPax)	Trial 1 (seven cells)	GaAs	2.31 ± 0.11		2.61 ± 0.08	
	Trial 2 (eight cells)	Flsn	2.48 ± 0.06		2.47 ± 0.06	
Double-exponential (GPax/FATmCh)	Trial 1 (seven cells)	GaAs	2.15 ± 0.12	0.01	2.51 ± 0.22	2.01 ± 0.14
	Trial 2 (seven cells)	Flsn	2.30 ± 0.10	0.01	2.56 ± 0.13	1.99 ± 0.08

To verify the conclusions drawn from fitting of cell data, single- and double-exponential decay curves were simulated (five sets of curves each). The single-exponential decay curves had a lifetime of 2.6 ns, and the double-exponential decay curves had lifetimes of $\tau_D = 2.6$ ns and $\tau_F = 1.3$ ns. The 2.6-ns lifetime was chosen because it is close to the nonFRET-ing lifetime of GFP, and a τ_D/τ_F ratio of 0.5 was chosen, giving $\tau_F = 1.3$ ns. The same fitting procedure as described above was carried out, with τ_D fixed at 2.6 ns for fit procedure (ii). The results are presented in Table 2.

When cell data are fit with single-exponential decays, global-indiv and segment-sum extract similar τ_D for the two cell populations each, with segment-sum values being slightly higher. For GPax cells, segment-sum recovered a lifetime of 2.58 ± 0.07 ns, whereas global-indiv recovered a lifetime of 2.47 ± 0.04 ns. Summing multiple single-exponential decay curves produces another single-exponential decay curve with the same lifetime but a higher photon count and less noise (higher SNR). For GPax/FATmCh cells, the value of τ_D is underestimated. When a double-exponential decay is force-fit with a single-exponential decay, an average lifetime of the actual two lifetimes present is recovered: 2.37 ± 0.10 ns from segment-sum and 2.30 ± 0.19 ns from global-indiv.

The results from simulated decay curves verified our conclusions. For single-exponential decays, segment-sum accurately extracted the lifetime, whereas global-indiv extracted a lifetime within 5% of the known value of 2.6 ns. This shows that global-indiv single-exponential fitting on curves with a single lifetime is affected by the SNR of the decay curves, but that fit results are not greatly compromised. For double-exponential decays, both methods extracted lifetimes within 10% of the average of the two true lifetimes.

Fits were also carried out by fixing τ_D to 2.6 ns. GPax cells are not expected to have two lifetimes. Segment-sum indeed recovers a second lifetime of 2.56 ± 0.06 ns, similar to the fixed τ_D value, indicating that it is possible to recover the single-decay lifetime even with a double-exponential fit from decay curves with very high SNR. Global-indiv is unable to recover the correct single lifetime because of the need for higher SNR data. It should be possible to recover the second lifetime present in GPax/FATmCh curves by fixing τ_D to the nonFRET lifetime value obtained from GPax cells. Fixing τ_D reduces the number of degrees of freedom given to the fitting algorithm, thus allowing the fits to converge faster. Segment-sum recovers a τ_F of 2.34 ± 0.12 ns, whereas global-indiv recovered a lower τ_F of 1.99 ± 0.05 .

The results from simulated decay curves verified our conclusions for single-exponential decays. For double-exponential decays, both segment-sum and global-indiv are able to recover the correct τ_F , to within 2%, though the segment-sum value is slightly more accurate. Though summing many double-exponential curves, each with its own fraction of the two lifetimes, averages over the prefactors in the fit equation, due to the very high resulting SNR in the summed decay, segment-sum is still well able to extract the known second lifetime. However, even though the extracted second lifetime obtained from segment-sum might be slightly more accurate, this method does not allow recovery of the prefactors. Therefore, global-indiv is the desired method for most applications. That the difference in lifetimes obtained from the two methods is larger for cell data compared to simulated data is an indication that experimental decay curves contain biological

Table 2 Lifetime fit results for cell and simulated data simulation data using various fitting procedures.

	GPax/single-exponential decays						GPax—FATmCh/double-exponential decays					
	Segment-sum		Global-indiv		FR		Segment-sum		Global-indiv		FR	
	τ_D (ns)	τ_F (ns)	τ_D (ns)	τ_F (ns)			τ_D (ns)	τ_F (ns)	τ_D (ns)	τ_F (ns)		
(i) Single-exponential fit	Cell data	2.58 ± 0.07		2.47 ± 0.04				2.37 ± 0.10		2.30 ± 0.19		
	Simulation data	2.58 ± 0.07		2.52 ± 0.00				2.15 ± 0.01		1.981 ± 0.00		
(ii) Double-exponential fit with τ_D fixed	Cell data	2.6	2.56 ± 0.06	2.6	2.05 ± 0.19	0.38 ± 0.25	2.6	2.34 ± 0.12	2.6	1.99 ± 0.05	0.51 ± 0.22	
	Simulation data	2.6	2.58 ± 0.01	2.6	2.00 ± 0.01	0.26 ± 0.29	2.6	1.30 ± 0.02	2.6	1.28 ± 0.01	0.52 ± 0.30	
(iii) Double-exponential fit	Cell data	2.59 ± 0.05	2.56 ± 0.04	2.76 ± 0.11	2.17 ± 0.08	0.49 ± 0.24	2.40 ± 0.10	2.33 ± 0.11	2.56 ± 0.13	1.99 ± 0.08	0.47 ± 0.24	
	Simulation data	2.60 ± 0.00	2.59 ± 0.01	3.02 ± 0.08	2.08 ± 0.01	0.54 ± 0.26	2.58 ± 0.05	1.29 ± 0.04	2.58 ± 0.01	1.27 ± 0.01	0.51 ± 0.30	

noise sources not accounted for when simulating decay curves only with Poisson noise.

When fits were carried out with both lifetimes free to vary, for GPax cells, segment-sum is again able to extract two lifetimes with similar values, 2.60 ± 0.05 ns and 2.56 ± 0.04 ns, because of the high SNR. However global-indiv fails and in fact recovers two distinctly different lifetimes due to the low SNR. The recovered values, 2.76 ± 0.11 ns and 2.17 ± 0.08 ns, lie on either side of the single lifetime present, and average to 2.47 ns, within 5% of 2.6 ns. For GPax/FATmCh decays, segment-sum also fails to recover the two expected lifetimes most likely because of the compound effect of averaging over the prefactors and because the two lifetimes present in the decay curves were not well-separated. Global-indiv, on the other hand, successfully recovered lifetimes of $\tau_D = 2.56 \pm 0.13$ ns and $\tau_F = 1.99 \pm 0.08$ ns.

The results from simulated decay curves again verified experimental results for single-exponential decays. Segment-sum extracted two lifetimes within 1% of the known τ_D , and global-indiv extracted two lifetimes well on either side of the known τ_D . This result shows that a false FRET detection can actually be deduced from single-exponential decays if these data are fit with double-exponential fits. It underscores the importance of exercising some discretion when applying mathematical methodology to known or expected biological phenomena. For double-exponential simulated curves, both segment-sum and global-indiv are able to recover the two lifetimes present in the curves within 5% error.

It is unclear which method is best to accurately determine recovered lifetimes when carrying out double-exponential fits on experimental cell data. Both lifetimes could be allowed to vary freely. However, fitted lifetimes may vary for images obtained in a single imaging session, as shown in Table 3. One way to overcome this uncertainty is to assume that τ_D is the same in both GPax-only and GPax/FATmCh cells. This assumption says that the lifetime of GPax in cells is the same, regardless of whether it is the sole fusion protein species within the cell or whether it is coexpressed with a partner fusion protein. For cells of the same type that are cultured, transfected, and imaged under the same conditions, this assumption is reasonable. By doing this, τ_D can be fixed when double-exponential fits are carried out, thus

recovering only τ_F and FR. With the use of this method, a comparison of the values of τ_F can be made across all images.

An important assumption underlying global analysis is the invariance of free and bound donor lifetimes within the cell. It is possible that different locations within the cell, delineated by varying fluorescence intensities, have microenvironments, such as protein aggregation state, protein phosphorylation state, and binding of cofactors, which may differentially affect the properties of fluorescent proteins. This would result in varying lifetimes, thus invalidating global analysis. Therefore, to test the validity of the global assumption on cell data, the double-exponential global analysis carried out on GPax-only cells as described above was further examined. Any variation between intensity regions would be apparent when looking at the FR distribution, even though the resultant lifetimes are artificial, because more fit parameters are allowed to vary. As can be seen in Fig. 3, however, FR distributes similarly, regardless of which intensity region is examined. This lack of intensity-dependent differences justifies the use of global analysis for our cell data.

As further validation, global analysis was carried out on pixels with similar intensities (and thus photon counts), but at different regions in the cell, either FAs or cytosol. Because FAs, as sites of cell attachment to the basal surface, transmit force and recruit a distinct set of proteins, these regions are morphologically and biologically different from the cytosol. It would be expected that if variations in fluorescent protein properties exist within the cell, comparing fit results from these two regions would extract such differences. Single-exponential fits carried out on these pixels retrieved $\tau_D = 2.65 \pm 0.03$ ns for FA pixels, and $\tau_D = 2.65 \pm 0.04$ ns for cytosolic pixels. There is indeed no difference between these lifetimes, which demonstrates the applicability of global analysis to cell data.

The choice of single exponential and biexponential fitting is partly motivated by the goal of finding the simplest models that can account for all the experimental observations. This choice is also partly justified by the limited number of photons in typical fluorescent images, and more complex models can rarely be distinguished, given Poisson statistics. We have demonstrated that paxillin-FAK binding is spatially invariant and that all

Table 3 Fit results for GPax and GPax/FATmCh cell data obtained during a single imaging session with two fitting procedures: (1) double-exponential fit with lifetimes free to vary and (2) double-exponential fit with τ_D fixed at 2.6 ns.

GPax (single-exponential fit)	Lifetimes free to vary			Fixed $\tau_D = 2.6$ ns		
	τ_D (ns)	τ_F (ns)	FR	τ_D (ns)	τ_F (ns)	FR
GPax/FATmCh 1	2.582	2.006	0.46 ± 0.22	2.6	2.010	0.50 ± 0.24
GPax/FATmCh 2	2.439	1.926	0.49 ± 0.24	2.6	1.952	0.60 ± 0.21
GPax/FATmCh 3	2.447	1.937	0.41 ± 0.23	2.6	1.970	0.55 ± 0.20
GPax/FATmCh 4	2.478	1.923	0.48 ± 0.24	2.6	1.942	0.57 ± 0.21
GPax/FATmCh 5	2.646	2.072	0.48 ± 0.23	2.6	2.062	0.44 ± 0.24
Mean	2.518	1.973			1.987	
s.d.	0.0091	0.065			0.049	

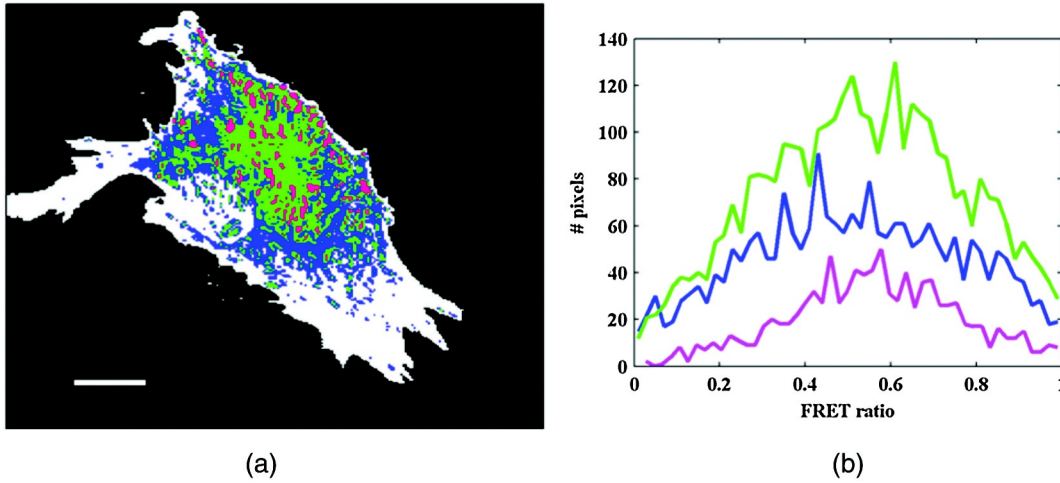


Fig. 3 (a) GPax cell segmented by intensity at LL1000. (b) Histogram of FR distribution of cell in (a), color-coded by cell intensity segment. A double-exponential fit was carried out to obtain the FR. Scale bar is 10 μm .

experimental data can be accounted for by one free donor lifetime and one bound donor lifetime. In other protein systems, this spatially invariant condition may not be valid, and different bound and free lifetimes may be associated with different cellular locations. Furthermore, different initial conditions used in global fitting may converge to different lifetimes and preexponential fractions. The choice of initial conditions has been discussed extensively in literature and is not examined in detail here.^{18,22,32,33,44}

Finally, although it is not the main focus of this work, it should be noted that the data model and the initial condition choices significantly affect whether a global fitting algorithm converges as well as the speed of convergence. Strategies to improve global algorithm efficiency have been previously developed.^{22,30,32–34,44,45}

4.3 Photon Counts Per Pixel: Lifetime Scaling

Typically, at least 100 counts per pixel are required to extract a lifetime with uncertainty of 20% from a fluorescence decay curve. A LL of 1000 counts per pixel is required to extract two lifetimes, provided the lifetimes are well-separated and the two prefactors are of comparable magnitude.^{21,33} In cell samples, these parameters cannot be predicted and depend entirely on the biological sample. The binding interaction between fusion proteins dictates the distance between FRETing fluorophores and thus τ_F . The expression rate of fusion proteins depends on the cell's transcription and translation machinery and cannot be controlled externally. Thus the FRET ratio (prefactors) distribution varies at each pixel, depending on the amount of fusion protein present. As we attempt to select cells that are not overexpressing fusion proteins, this limits the total photon counts that can be collected within each pixel, where it might be difficult to collect even 1000 counts per pixel for a two-lifetime fit. Moreover, our fusion proteins localize to FAs, leading to a difference in pixel intensity between FA and cytosolic regions. Whereas FAs might contain pixels with more than 1000 counts, cytosolic regions might not.

To overcome these limitations, we examined how the fitted lifetimes and FRs deviate with varying LLs on photon counts for GPax/FATmCh cells. For GPax cells, this process is unnecessary because enough pixels per cell have counts higher than 1000. Besides, segment-sum adequately recovers the true τ_D from

single-exponential decay curves, as previously shown. For GPax/FATmCh cells, τ_D was fixed at 2.6 ns, whereas τ_F and FR were recovered by carrying out fits at varying photon count LL values corresponding to the total number of integrated photons under a decay curve. Figure 4(a) shows representative double-exponential fits carried out with τ_D fixed at 2.6 ns for two sets of data corresponding to measured cell simulation. The open circles in Fig. 4(b) show the variation in fitted τ_F with LL. The fitted τ_F reaches a plateau at LL of ≈ 1500 . Fits carried out on simulated curves with a τ_F/τ_D ratio of 0.8 and varying LL show similar trends (closed circles). This dependence on LL can also be seen by quantifying the percentage deviation from plateau value, it can be seen that the curves from both cells (open triangles) coincide, with the curve from simulated data (closed triangles) following a similar trend. Inclusion of decay curves with lower-intensity cell data (low LL) into fits leads to systematic underestimation of the second lifetime present in the double-exponential decays. Because the deviation with LL is systematic, it should be possible to carry out fits at lower LL to include as many pixels as possible from cell data, including dimmer pixels, and apply a correction factor to pixels with lower LL. To map out this systematic variation, fits were carried out on simulated curves at varying LL and τ_F/τ_D ratios.

Trends in percentage deviation in fit τ_F with τ_F/τ_D ratio are shown in Fig. 4(c), where the known τ_F is used when calculating τ_F/τ_D . Percentage deviation, such as that between LL500 and LL2000, is defined as follows:

$$\frac{\tau_{F(LL500)} - \tau_{F(LL2000)}}{\tau_{F(LL2000)}} \cdot 100. \quad (5)$$

Hereafter it is written as 500%dev2000. Squares are percentage deviation from $\tau_{F(LL2000)}$ (500%dev2000 and 1000%dev2000), circles are percentage deviation from $\tau_{F(LL2000)}$ (500%dev1000), and triangles are percentage deviation from known τ_F (500%dev τ_F , 1000%dev τ_F , and 2000%dev τ_F). Dotted lines are fits of LL500 %dev points, dashed lines are fits of LL1000 %dev points, and the solid line is a fit of LL2000 %dev points. The τ_F obtained from fits with LL2000 is very close to the true τ_F , within 10% for lifetime ratios between 0.02 and 0.82. However, as previously mentioned, the lifetime is increasingly underestimated with higher τ_F/τ_D ratio. Although initially LL1000 was the minimum criteria for obtaining

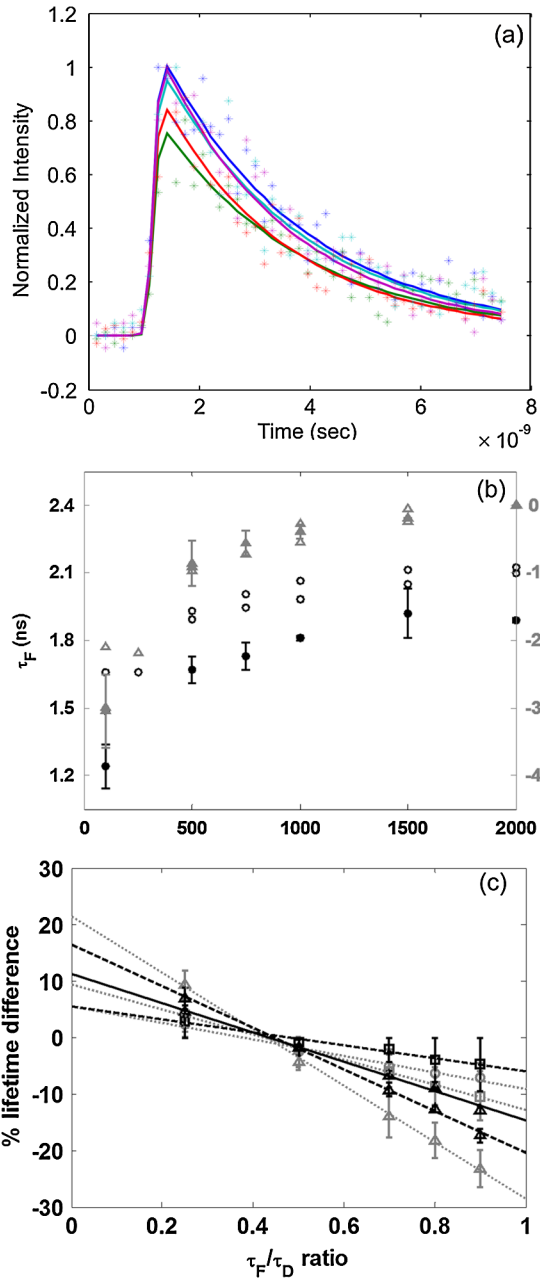


Fig. 4 Double-exponential fits were carried out with τ_D fixed at 2.6 ns for both cell and simulated data. (a) Lifetime decay data and the associated curve fits for five representative pixels of the LL100 data set (containing 1458 pixels in total) are shown. The normalized χ^2 for fitting the whole data set is 0.26 without reweighting and is 0.67 with reweighting (see also Table 5). (b) Variation in fitted τ_F with varying LL. Left axis is fitted τ_F (circle) right axis is percentage difference in fitted τ_F compared to fitted τ_F at LL2000 (triangle). Open markers: two independent cell measurements; closed markers: simulated data. (c) Master curve for scaling τ_F fit to true τ_F . Squares are percentage deviations from τ_F (LL2000) (500%dev2000 and 1000%dev2000), circles are percentage deviations from τ_F (LL1000) (500%dev1000), and triangles are percentage deviations from true τ_F (500%dev τ_F , 1000%dev τ_F , and 2000%dev τ_F). Dotted lines are fits of LL500 %dev points, dashed lines are fits of LL1000 %dev points, and solid line is a fit of LL2000 %dev points.

“good fits,” Fig. 4(c) shows that results obtained from LL1000 fits can in fact be scaled up to the true value. Thus Fig. 4(c) provides the τ_F master curve generated from linear regressions of simulation data, from which the value of the true τ_F can be

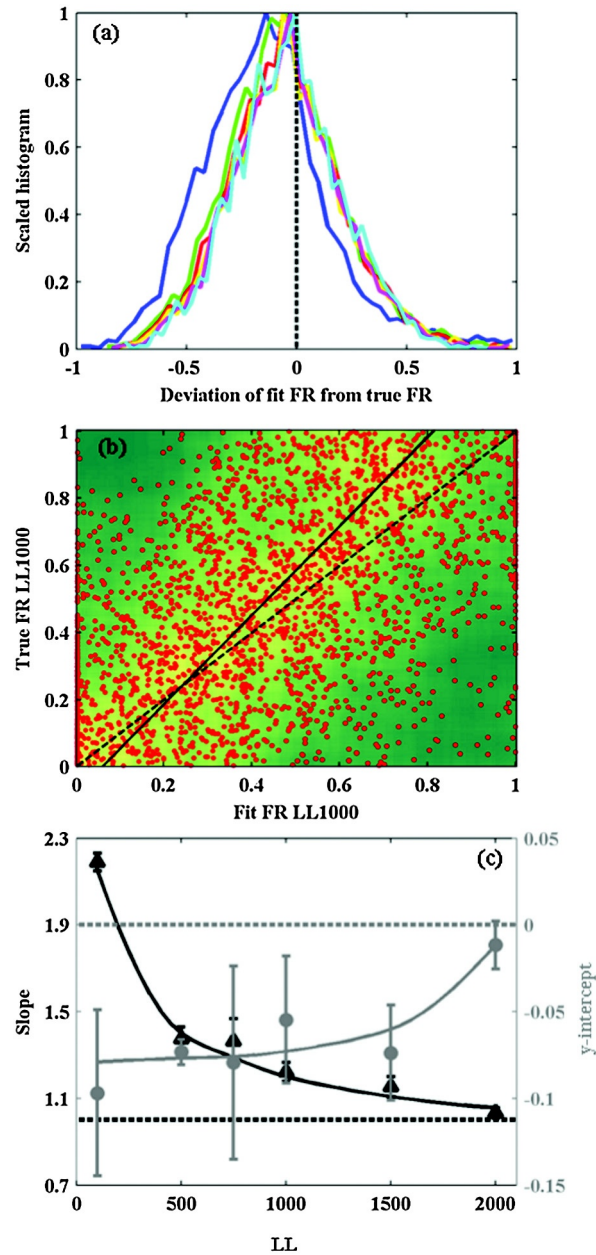


Fig. 5 (a) Scaled histogram of fit-truFR at τ_F/τ_D ratio of 0.8 and varying LL values. Color scheme is as follows: LL100 (dark blue), LL500 (green), LL750 (red), LL1000 (yellow), LL1500 (magenta), and LL2000 (light blue). (b) Plot of true FR versus fit FR at τ_F/τ_D ratio of 0.8 and LL1000. Red points: raw data. Plot is pseudocolored by data density; yellow: high density of data; green: low density of data, with a gradation for intermediate values. Solid line: line of best fit through data, dashed line: line with 0 y-intercept and slope of 1. (c) Slope (triangle) and intercept (circle) of true versus fitted FR plots at τ_F/τ_D ratio of 0.8 and with varying LL. A best-fit line is drawn through the data points based on a third-degree spline fit (using polyfit function of MATLAB) to generate a master curve.

determined for fits at any LL. As an example, for cell data, fits can be carried out at any two LL values, at LL500 to include most of the pixels within cells and at LL1000 to capture a smaller fraction of the pixels. The percentage deviation, 500%dev1000, can be calculated from the fitted τ_F obtained at these two LL values. Referring to the 500%dev1000 master curve, the true τ_F/τ_D ratio can be read from the x-axis.

This plot corroborates finding in literature that a minimum of LL1000 is sufficient to extract τ_F within 20% of the true value.

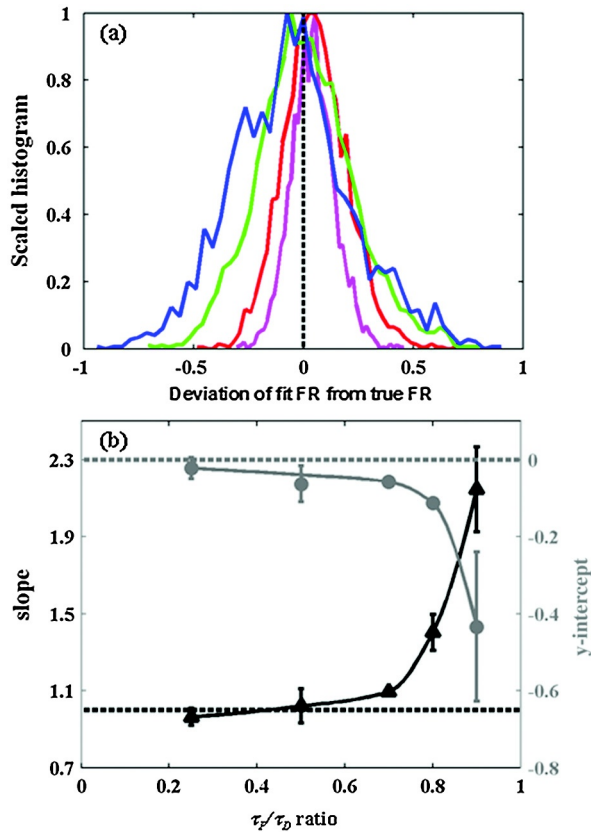


Fig. 6 (a) Scaled histogram of fit-truFR at LL1000 and varying τ_F/τ_D ratio. Color scheme is as follows: $\tau_F/\tau_D = 0.25$ (magenta), $\tau_F/\tau_D = 0.5$ (red), $\tau_F/\tau_D = 0.7$ (green), $\tau_F/\tau_D = 0.8$ (blue). (b) Slope and intercept of true versus fit FR plots at LL1000 and varying τ_F/τ_D ratio. A best-fit spline is drawn through the data points.

However, we can actually scale the fitted lifetime to the true τ_F , enabling us to calculate a more accurate value for FRET efficiency and thus interfluorophore distance, r . The ability to use pixel with lower photon counts further allows us to study regions where fluorescent protein expression is lower.

Though much effort has previously been put into analyzing the accuracy of fitted lifetime values obtained from FLIM data, not much work has been done to examine the variations in the exponential prefactors with various fitting protocols. In this study, we examined the effect of variations in τ_F/τ_D and LL on prefactors, formulated as FR, as previously described.

Fits were carried out at $\tau_F/\tau_D = 0.8$ and varying LL. A scaled histogram of the difference in fit compared to true FR (fitFR - truFR) is shown in Fig. 5(b). The histogram is similar for all LL values except LL100. This is very likely because at LL100, the SNR is below the threshold for obtaining reasonable fit parameters. The histogram is not quite symmetrical about 0 deviation, but is skewed slightly toward negative deviation. A plot of true FR against fit FR at LL1000 [Fig. 5(c)] shows the actual distribution of FR values via a linear regression. For comparison, a dashed line with zero y-intercept and slope of 1 is also plotted. A fit that produces results with a symmetrical histogram about 0 deviation would produce a true FR versus fit FR plot with data points scattered about this line. The open circles show the position where the points are most dense (histogram peak). When a line of best fit is drawn through the circles, the parameters recovered are a y-intercept of -0.12 and slope of 1.5. If a cell data fit were carried out at LL1000 and the τ_F/τ_D ratio was found to be 0.8 by scaling from the τ_F master curve, the slope and y-intercept values would be used to shift fit FR values to true FR values. Figure 5(c) is a plot of slope and intercept for fits at a τ_F/τ_D ratio of 0.8 and varying LL. It shows that the slope approaches 1 and the y-intercept approaches 0 with higher LL. This is an obvious trend, as decays with higher total counts have better SNR, leading to more accurate fits.

A scaled histogram of fit-truFR at LL1000, with varying τ_F/τ_D ratios, shows more pronounced differences between low lifetime ratios and higher lifetime ratios [Fig. 6(a)]. The histogram skews from more positive differences to more negative differences with increasing τ_F/τ_D ratios. Besides that, relatively more pixels show higher differences with increasing τ_F/τ_D ratios. We can again plot the variation in slope and y-intercept with varying ratios, and the plot shows that the slope approaches 1 and the y-intercept approaches 0 as τ_F/τ_D decreases [Fig. 6(b)]. This suggests that FR can be extracted more accurately from FLIM data when the lifetimes are more widely separated.

With each variation in lifetime ratio and LL, it is possible to deterministically calculate the variation in fit FR. Therefore, it is possible to scale parameters obtained from low LL to true lifetime and FR, based on the slope and y-intercept values presented here. Conversely, it is possible to state the variance in true FR at any fit FR value.

It is interesting to examine the underlying reason for the systematic underestimation of the lifetime of the short component and the FRET ratio with lower photon counts. That is to say, for

Table 4 Fit results for a single-decay curve with high photon counts when curves with increasingly lower LL values are included in the fit.

	Fix $\tau_D = 2.6$ ns		Intersection of fit at LL2000 with fit at LL values		Lifetimes free to vary		
	τ_F (ns)	FR	x-axis: time (ns)	y-axis: No. of photons	τ_D (ns)	τ_F (ns)	FR
LL2000	1.897	0.885					
LL1500	1.864	0.845	5.994	44.118	2.75	1.884	0.893
LL1000	1.808	0.787	5.970	44.420			
LL750	1.765	0.747	5.951	44.673			
LL500	1.690	0.687	5.917	45.147			
LL100	1.247	0.474	5.654	48.969			

Table 5 Comparison of lifetimes recovered using weighting method with master curve lookup.

Fix $\tau_D = 2.6$ ns	τ_F (Least squares)	τ_F (Reweighting)	τ_F (Master curve)
LL50	1.64	1.82	
LL100	1.70	1.86	
LL500	1.79	1.91	1.87 ^a , 1.77 ^b
LL1000	1.84	1.87	1.82 ^c
LL2000	1.92	1.87	

^a500%dev1000.^b500%dev1000.^c1000%dev2000.

any given decay curve with high photon count, including decay curves with progressively lower photon counts in the fit, τ_F shifts for the whole set of curves to lower values and FR for that decay curve also falls (Table 4). The origin of this underestimation is due to fitting the decay curves using a least-squares function that is an unbiased estimator only for Gaussian noise, whereas the decay curves are dominated by Poisson noise. This behavior can be attributed to the presence of a noise floor. With the lifetime of the long component fixed and fitting to the noise floor at the longer time, the minimization of χ^2 results in an overestimation of long lifetime component amplitude that is compensated by a reduction of the short component lifetime and the FRET ratio.

An alternative reweighting method to compensate for this bias in least-squares fitting has been developed by Selinger and co-workers and recently by Truton and co-workers.⁴⁶⁻⁴⁸ It has been shown that using a modified χ^2 weighted error function consisting of the values of the fitted curve (instead of the values of the data) in the final fitting step can effectively remove fitting bias. We have adopted this method to analyze some of our simulated data and compared the results with our reference master curve approach. The results are shown in Table 5, and we found that both methods allow recovery of the correct τ_F , providing a cross-validation of our approach.

5 Discussion

On the basis of the results we have presented, a data analysis protocol followed for a particular imaging session can be formulated thus:

1. Carry out single-exponential decay fits on GPax cells.
2. Calculate the mean of fitted τ_D s and use this value as the fixed τ_D when carrying out double-exponential decay fits on GPax/FATmCh cells.
3. Recover τ_F and FR distributions from fits on GPax/FATmCh cells at different LLs.
4. Scale τ_F and FR from fit to true values using master curves.

Single-exponential decay fits were carried out on six GPax cells' decay curves. The single lifetime extracted was 2.68 ± 0.07 ns. Thus a τ_D of 2.7 ns was used as the fixed value when carrying out double-exponential decay fits on six

GPax/FATmCh cells' decay curves. Double-exponential decay fits were carried out at LL500, LL1000, and LL2000 for comparison. Percentage deviations 500%dev1000, 500%dev2000, and 1000%dev2000 were calculated. On the basis of the FR

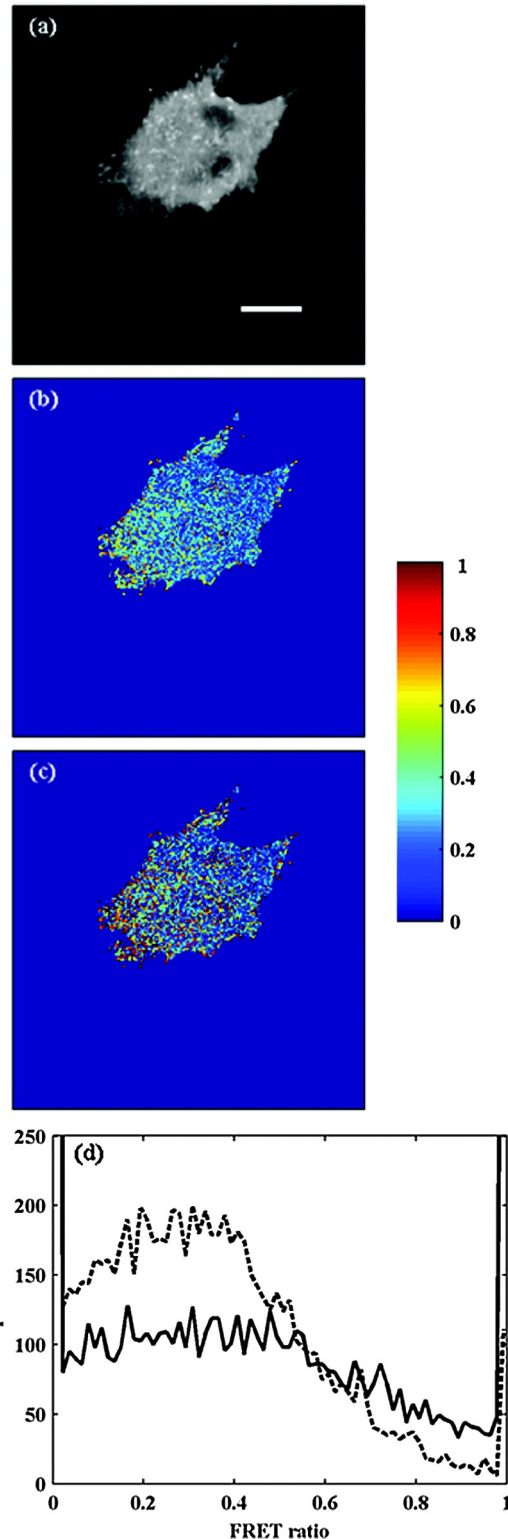


Fig. 7 (a) Intensity image of GPax/FATmCh cell. (b) Cell image pseudocolored by fit FRET ratio. (c) Cell image pseudocolored by scaled FRET ratio. (d) Histogram of FRET ratio. Dotted line: fit FR, solid line: scaled FR. Scale bar is 10 μ m.

master curve, these %devs correspond to a ratio of true τ_F/τ_D of 0.83 ± 0.07 . The true τ_F is thus calculated to be 2.24 ± 0.08 ns. This lifetime value can be cross-checked by using the %dev τ_F master curves. From this, a lifetime value of 2.37 ± 0.16 ns is obtained, giving an accuracy of 6% to our τ_F estimate. From these calculations, the FRET efficiency of GPax and FATmCh in our intracellular system is 17%, translating to an interfluorophore distance of 61.3 Å.

The fit FR was scaled using slope and intercept values of 1.715 and -0.174 respectively. These were obtained from a fit versus true FR plot at $\tau_F/\tau_D = 0.85$ and LL1000 (data not shown). The result of scaling FR is shown in Fig. 7. Figure 7(a) is an fluorescence intensity image of a GPax/FATmCh cell. Figure 7(b) shows the same cell pseudocolored by the fit FR, and Fig. 7(c) shows the cell pseudocolored by the scaled FR. A histogram of fit FR and scaled FR shows the redistribution of FR upon scaling [Fig. 7(d)]. Thus, on the basis of our scaling methodology, we were able to carry out fits on cell data with lower intensities and scale the resulting lifetime and FR to true values based on a set of master curves.

6 Conclusions

For our model system of interacting GPax and FATmCh proteins within BAECs, we have shown that when the IR varies throughout the imaging session, it is not possible to use an IR measured at the start of the session to fit data from the whole session. An adaptive method is instead used to directly extract an IR from the experimental TCSPC data.

By systematically tracking the variation in lifetime and FR when the known τ_D is fixed for double-exponential decay fits on simulated curves, we were able to generate lifetime and FR master curves. This allows cell data with low photon counts to be included in the fitting procedure. The resulting fit parameters (lifetime and FR) can be scaled to true values using the master curves. This overcomes the need to carry out fits only with high photon counts, as has been previously shown by other groups, and allows us to obtain more information from dim regions of the cell that previously would have had to be neglected.

By assuming that the GPax lifetime in cells is the same regardless of whether another fluorophore is present, a step-by-step method can be used to obtain FRETing lifetimes from double-transfected cells. Fits of decay curves from GPax-only cells provide this lifetime, which is then fixed for analysis of double-exponential curves from GPax/FATmCh cells. The results are then scaled using the previously mentioned master curves. This methodical process is important to drawing conclusions based on real experimental cell data, where photon counts cannot be externally controlled and are necessarily low.

It should be noted that several important assumptions must be made for this methodology to be valid. First is the assumption that only free and bound donor fluorescence are measured. Complicating factors such as cellular autofluorescence and acceptor fluorescence are negligible. Second, it is important that the donor lifetime, such as GFP used in this study, is substantially single-exponential. Donor fluorophores with more complex decay dynamics may substantially complicate FRET analysis. Third, free donor lifetime is invariant within the cell. Factors such as protein aggregation and quenching do not affect donor lifetime. Fourth, the conformation of donor-acceptor of bound protein is invariant within the cell, and the decay curves within the cell can be accurately modeled as a biexponential

decay. However, it should be noted that these restrictions may be partly restricted if they are valid within regions of the cell and these regions can be selected for analysis based on image segmentation. Finally, other factors such as photobleaching are also assumed to be negligible.

Acknowledgments

We thank K. Yamada of the National Institutes of Health, Bethesda, MD, for his kind gift of GFP-paxillin plasmid; N. Mochizuki of the Department of Structural Analysis, National Cardiovascular Center Research Institute, Osaka, Japan, for his kind gift of dsRed-FAT plasmid; and R. Tsien of the Department of Pharmacology, Department of Chemistry & Biochemistry, University of California San Diego, San Diego, CA. We also gratefully acknowledge the technical assistance of A. Sieminski (Olin College), P. Patwari (Brigham & Women's Hospital (BWH)) and P. C. Schulze (BWH). This study was supported in part by National Heart, Lung, and Blood Institute grant HL-64858. P. So and R. Kamm recognize support from the Singapore MIT Alliance for Research and Technology Center (SMART). P. So further recognizes support from Singapore-MIT Alliance 2 (SMA2).

References

1. R. Y. Tsien, "The green fluorescent protein," *Annu. Rev. Biochem.* **67**, 509–544 (1998).
2. M. E. Bulina et al., "A genetically encoded photosensitizer," *Nat. Biotechnol.* **24**(1), 95–99 (2006).
3. D. M. Chudakov, S. Lukyanov, and K. A. Lukyanov, "Fluorescent proteins as a toolkit for in vivo imaging," *Trends Biotechnol.* **23**(12), 605–613 (2005).
4. X. Shu et al., "Novel chromophores and buried charges control color in mFruits," *Biochemistry* **45**(32), 9639–9647 (2006).
5. H. W. Ai et al., "Exploration of new chromophore structures leads to the identification of improved blue fluorescent proteins," *Biochemistry* **46**(20), 5904–5910 (2007).
6. H. Chen et al., "Measurement of FRET efficiency and ratio of donor to acceptor concentration in living cells," *Biophys. J.* **91**(5), L39–L41 (2006).
7. C. Berney and G. Danuser, "FRET or no FRET: a quantitative comparison," *Biophys. J.* **84**(6), 3992–4010 (2003).
8. T. Zal and N. R. Gascoigne, "Photobleaching-corrected FRET efficiency imaging of live cells," *Biophys. J.* **86**(6), 3923–3939 (2004).
9. E. B. Van Munster et al., "Fluorescence resonance energy transfer (FRET) measurement by gradual acceptor photobleaching," *J. Microsc.* **218**(Pt. 3), 253–262 (2005).
10. T. Haraguchi et al., "Spectral imaging fluorescence microscopy," *Genes Cells* **7**(9), 881–887 (2002).
11. C. Thaler et al., "Quantitative multiphoton spectral imaging and its use for measuring resonance energy transfer," *Biophys. J.* **89**(4), 2736–2749 (2005).
12. C. Biskup et al., "Multi-dimensional fluorescence lifetime and FRET measurements," *Microsc. Res. Technol.* **70**(5), 442–451 (2007).
13. A. L. Mattheyses, A. D. Hoppe, and D. Axelrod, "Polarized fluorescence resonance energy transfer microscopy," *Biophys. J.* **87**(4), 2787–2797 (2004).
14. K. A. Lidke et al., "The role of photon statistics in fluorescence anisotropy imaging," *IEEE Trans. Image Process.* **14**(9), 1237–1245 (2005).
15. M. Cohen-Kashi, Y. Namer, and M. Deutsch, "Fluorescence resonance energy transfer imaging via fluorescence polarization measurement," *J. Biomed. Opt.* **11**(3), 034015 (2006).
16. M. A. Rizzo and D. W. Piston, "High-contrast imaging of fluorescent protein FRET by fluorescence polarization microscopy," *Biophys. J.* **88**(2), L14–L16 (2005).
17. V. Ghukasyan et al., "Application of fluorescence resonance energy transfer resolved by fluorescence lifetime imaging microscopy for

- the detection of enterovirus 71 infection in cells," *J. Biomed. Opt.* **12**(2), 024016 (2007).
18. S. Pelet, M. J. Prevlite, and P. T. So, "Comparing the quantification of Forster resonance energy transfer measurement accuracies based on intensity, spectral, and lifetime imaging," *J. Biomed. Opt.* **11**(3), 034017 (2006).
 19. S. Pelet et al., "Spectrally resolved lifetime imaging to quantify Fluorescence Resonant Energy Transfer (FRET) in a two-photon microscope," *Biophys. J.* **88**(1), 339a–339a (2005).
 20. M. Millington et al., "High-precision FLIM-FRET in fixed and living cells reveals heterogeneity in a simple CFP-YFP fusion protein," *Biophys. Chem.* **127**(3), 155–164 (2007).
 21. E. Gratton et al., "Fluorescence lifetime imaging for the two-photon microscope: time-domain and frequency-domain methods," *J. Biomed. Opt.* **8**(3), 381–390 (2003).
 22. P. J. Verwee and P. I. Bastiaens, "Evaluation of global analysis algorithms for single frequency fluorescence lifetime imaging microscopy data," *J. Microsc.* **209**(Pt. 1), 1–7 (2003).
 23. A. H. Clayton, Q. S. Hanley, and P. J. Verwee, "Graphical representation and multicomponent analysis of single-frequency fluorescence lifetime imaging microscopy data," *J. Microsc.* **213**(Pt. 1), 1–5 (2004).
 24. F. Festy et al., "Imaging proteins in vivo using fluorescence lifetime microscopy," *Mol. Biosyst.* **3**(6), 381–391 (2007).
 25. H. Wallrabe and A. Periasamy, "Imaging protein molecules using FRET and FLIM microscopy," *Curr. Opin. Biotechnol.* **16**(1), 19–27 (2005).
 26. S. S. Vogel, C. Thaler, and S. V. Koushik, "Fanciful FRET," *Sci. STKE* **2006**(331), 19–27 (2006).
 27. J. R. Alcala, E. Gratton, and F. G. Prendergast, "Resolvability of fluorescence lifetime distributions using phase fluorometry," *Biophys. J.* **51**(4), 587–596 (1987).
 28. J. R. Alcala, E. Gratton, and F. G. Prendergast, "Fluorescence lifetime distributions in proteins," *Biophys. J.* **51**(4), 597–604 (1987).
 29. L. J. Libertini and E. W. Small, "Application of method of moments analysis to fluorescence decay lifetime distributions," *Biophys. Chem.* **34**(3), 269–282 (1989).
 30. G. C. Malachowski, R. M. Clegg, and G. I. Redford, "Analytic solutions to modelling exponential and harmonic functions using Chebyshev polynomials: fitting frequency-domain lifetime images with photobleaching," *J. Microsc.* **228**(Pt. 3), 282–295 (2007).
 31. M. A. Digman et al., "The phasor approach to fluorescence lifetime imaging analysis," *Biophys. J.* **94**(2), L14–L16 (2008).
 32. P. J. Verwee, A. Squire, and P. I. Bastiaens, "Global analysis of fluorescence lifetime imaging microscopy data," *Biophys. J.* **78**(4), 2127–2137 (2000).
 33. S. Pelet et al., "A fast global fitting algorithm for fluorescence lifetime imaging microscopy based on image segmentation," *Biophys. J.* **87**(4), 2807–2817 (2004).
 34. C. Buranachai et al., "Rapid frequency-domain FLIM spinning disk confocal microscope: lifetime resolution, image improvement and wavelet analysis," *J. Fluoresc.* **18**(5), 929–942 (2008).
 35. P. Wu and L. Brand, "Resonance energy transfer: methods and applications," *Anal. Biochem.* **218**(1), 1–13 (1994).
 36. G. H. Patterson, D. W. Piston, and B. G. Barisas, "Forster distances between green fluorescent protein pairs," *Anal. Biochem.* **284**(2), 438–440 (2000).
 37. P. T. So et al., "Two-photon excitation fluorescence microscopy," *Annu. Rev. Biomed. Eng.* **2**, 399–429 (2000).
 38. N. Klonis et al., "Spectral properties of fluorescein in solvent-water mixtures: applications as a probe of hydrogen bonding environments in biological systems," *Photochem. Photobiol.* **67**(5), 500–510 (1998).
 39. L. M. Edelman, R. Cheong, and J. D. Kahn, "Fluorescence resonance energy transfer over approximately 130 basepairs in hyperstable lac repressor-DNA loops," *Biophys. J.* **84**(2 Pt. 1), 1131–1145 (2003).
 40. J. E. Lofroth, "Deconvolution of single photon counting data with a reference method and global analysis," *Eur. Biophys. J.* **13**(1), (45–58 (1985).
 41. M. Ameloot, J. M. Beechem, and L. Brand, "Simultaneous analysis of multiple fluorescence decay curves by Laplace transforms. Deconvolution with reference or excitation profiles," *Biophys. Chem.* **23**(3–4), 155–171 (1986).
 42. L. J. Libertini and E. W. Small, "F/F deconvolution of fluorescence decay data," *Anal. Biochem.* **138**(2), 314–318 (1984).
 43. M. Zuker et al., "Delta function convolution method (DFCM) for fluorescence decay experiments," *Rev. Sci. Instr.* **56**(1), 14–22 (1985).
 44. P. J. Verwee, A. Squire, and P. I. Bastiaens, "Improved spatial discrimination of protein reaction states in cells by global analysis and deconvolution of fluorescence lifetime imaging microscopy data," *J. Microsc.* **202**(Pt. 3), 451–456 (2001).
 45. D. G. Walbridge, J. R. Knutson, and L. Brand, "Nanosecond time-resolved fluorescence measurements during protein denaturation," *Anal. Biochem.* **161**(2), 467–478 (1987).
 46. B. E. Saleh and B. K. Selinger, "Performance of single photon decay spectrometers with pile-up correction," *Appl. Opt.* **16**(5), 1408–1411 (1977).
 47. P. Hall and B. K. Selinger, "Better Estimates of Exponential Decay Parameters," *J. Phys. Chem.* **85**(20), (2941–2946 (1981).
 48. D. A. Turton, G. D. Reid, and G. S. Beddard, "Accurate analysis of fluorescence decays from single molecules in photon counting experiments," *Anal. Chem.* **75**(16), 4182–4187 (2003).